Sparse and specific somatosensory functional innervation of dorsolateral striatal neurons

Kenza Amroune, Lorenzo Fontolan, David Robbe, Ingrid Bureau

Sparse and specific somatosensory functional innervation of dorsolateral striatal neurons

Kenza Amroune[1], Lorenzo Fontolan[2], David Robbe[2] and Ingrid Bureau[1]*

[1] Aix-Marseille Université, INSERM, INMED, Marseille, France

[2] Aix-Marseille Université, INSERM, INMED, Turing Centre for Living Systems, Marseille, France

* corresponding author

Summary

The dorsal striatum receives dense and overlapping cortical projections making it an important structure for sensory integration. However, the degree of input convergence to individual striatal projection neurons (SPNs) is unclear. To address this issue, we investigated convergence in the vibrissal corticostriatal projection using an *ex vivo* functional approach combining laser scanning photostimulation in the mouse barrel cortex with patch-clamp recordings in the dorsolateral striatum. We found that the functional innervation of individual SPNs is sparse and specific to each cell, suggesting that sensory integration occurs at the population level. However, patterns with different degrees of input convergence were observed. Interestingly, they are associated with intrinsic behavioral biases of mice placed in an open field: preference for contralateral tactile input for direct pathway SPNs and locomotion speed for indirect pathway SPNs. Altogether, these results suggest that corticostriatal connections are selectively formed, constraining the convergence of vibrissal input to each SPN and generating innervation patterns that reflect individual biases in tactile behavior.

Highlights

- Functional mapping of cortical cells targeting striatal projection neurons
- Projections from barrel cortex to single SPNs are sparse and cell-specific
- Input convergence tuned to the biases of mice when sampling tactile information
- Lateralization in the direct pathway; Velocity in the indirect pathway

Introduction

An important feature of models of basal ganglia functions is that cortical inputs are sent through multiple overlapping channels such that striatal neurons may integrate sensorimotor, cognitive and limbic signals [1,2]. In the dorsal striatum, this diffuse organization of cortical projections has been supported by anatomical studies showing that, although sensory regions could be delineated, their boundaries were loose and fibers from different cortical areas overlapped [3–8]. Indeed, tracing of projections from domains in sensory and motor cortex revealed overlaps, the extent of which depended on the distance between areas and their interconnectivity [3,4,9,10]. Functional observations have also supported the loose topographic organization of corticostriatal projections, describing interspersed clusters of neurons along a recording electrode placed in the dorsolateral striatum (DLS) that respond to sensory stimulation or movement of different parts of the body [11–14]. However, these studies also revealed that, counterintuitively, each neuron in the DLS responded to a single body part (e.g., neck or whiskers or limb…) [11–13,15]. These observations suggest an innervation model in which each SPN in the DLS selectively receives connections from a small region of the somatosensory cortex, despite the availability of a larger panel of sensory projections. However, the degree of input convergence to individual cells revealed by electrophysiology may vary depending on whether spiking units or subthreshold responses are recorded, or whether animals are anesthetized or engaged in a task. Thus, the extent to which sensory inputs converge on individual SPNs remains unclear. In addition, patterns of innervation may also be cell specific. Indeed, SPNs are segregated into two pathways, termed direct and indirect, whose organization allows for differential regulation of basal ganglia output neurons [16–19]. It was previously described that inputs received by the dopamine receptor (DR)-1-expressing SPNs in the direct pathway are stronger than those received by the DR2-expressing SPNs in the indirect pathway [15,20–23] (neurons are hereafter referred to as D1 and D2 SPNs). Finally, patterns of innervation on SPNs may differ between individuals to support or adapt to different sensory integration capabilities. Rodents show individual behavioral biases when exploring a novel environment. First, they are spontaneously lateralized, preferentially exposing one side of their body and whiskers to sample tactile input as they move along walls (a behavior called thigmotaxis)[16,24]. Second, rodents move in an open field with an individual-specific overall speed (or distance traveled) [25,26]. These two features of their behavior, side preference and velocity, are sensitive to manipulations at the level of the whiskers or barrel cortex, which alter tactile and egomotion perception, and at the level of the striatum [24,27–33]. Based on these observations, it has been hypothesized that individualities in these behaviors are indicative of variations

in the properties of sensorimotor integrating circuits. Ultimately, stronger and broader sensory innervation to individual SPNs may be two of these properties.

To characterize the pattern of the vibrissal corticostriatal projections, we used the functional mapping technique for brain slices that combined patch-clamp recordings in the DLS with laser scanning photostimulation (LSPS) for stimulating neurons in the barrel cortex. The locations in the cortex where LSPS evoke synaptic currents indicate the locations of neurons that are presynaptic to the SPN being recorded. We found that cortical neurons innervating a SPN are sparse, and sometimes scattered over large regions of the barrel field. SPNs were innervated by one or a few whisker columns, and shared few inputs even when they were close together. These findings support the model that sensory integration occurs primarily at the population level rather than at the level of single cells in the DLS. Overall, D1 and D2 SPNs had similar innervation. But, by comparing the pattern of SPN innervation with the behavior of mice during thigmotaxis, we uncovered that D1 SPN vibrissal innervation was enhanced if mice showed a preference for contralateral tactile inputs. In contrast, the pattern of D2 SPN innervation was related to the animal velocity, as inputs from spatially distant whisker cortical columns converged on these cells in animals with faster displacements.

Results

General organization of the projections from the barrel cortex to the dorsal striatum

To study the spatial organization of the sensory projections onto SPNs functionally, we prepared corticostriatal slices from Drd1a-tdTomato hemizygous mice (PND 22-43; Fig. 1A and Supplemental Fig. 1A) and recorded $Drd1^+$ and $Drd1^-$ SPNs in the DLS in the whole cell voltage–clamp configuration (n = 101 cells, N = 54 mice). Simultaneously, an ultraviolet laser beam was directed at every site of a 29 x 16 pixel grid (2.1 × 1.1 mm), uncaging glutamate over the barrel cortex, exciting cortical neurons, and revealing glutamatergic cells presynaptic to the recorded SPN (Fig. 1A-B). When glutamate was uncaged on a cortical neuron innervating the recorded SPN, photo-stimulation elicited short-lived excitatory postsynaptic currents (EPSCs; < 50 ms duration) (Fig. 1B). We and others have shown that EPSCs are mono-synaptically evoked in our conditions, because only subthreshold events are elicited [34,35] (Supplemental Fig. 1B). For each cell, a so-called input map was assembled from the responses evoked at each uncaging site of the LSPS grid (Fig. 1C). Generally, multiple stimulated sites evoked EPSCs in a SPN. These ''connected sites'' were either adjacent or separated by non-connected sites in the barrel cortex.

As previously described [23,36,37], the layer (L) 5a was the principal source of innervations to SPNs in the dorsal striatum, as ~ 65% of them received input from this layer (Fig. 1D). Responses were elicited less frequently when stimulations were in L4, L5b, L2/3 and in L6 [23,38,39]. We tested whether the depolarizations caused by the uncaging of glutamate over the apical dendrites of L5a cells evoked action potentials, as this would make the distinction between the stimulation of L4 or L2/3 cells and L5 cells harder. We found that 50 % of L5a cells fired action potentials when stimulations were at the bottom of L4, indicating that a fraction of the L4-inputs were in fact due to the activation of L5 pyramidal cells (Supplemental Fig. 1B,D). In contrast, photo-stimulations in L2/3 never elicited the firing of L5a cells (n = 11; Supplemental Fig. 1B), indicating that the EPSCs evoked by stimulations in these superficial layers all arise from direct synaptic connections between L2/3 pyramidal cells and SPNs [23,40]. EPSCs evoked with stimulations in L2/3 to L5b had similar amplitudes (Fig. 1E), suggesting that L5a dominated the other layers through a denser innervation of SPNs principally. However, L6-EPSCs were smaller compared to L5a-EPSCs (Fig1. E, Kruskal-Wallis, $H(4) = 21.09$, $p = 0.0003$; Dunn-Šidák posthoc test, $p = 0.0003$).

To investigate the organization of the corticostriatal projection along the axis of barrels, we superposed the SPN input maps all aligned with respect to the same landmarks in the slice (see Methods), and color coded each site with input in the barrel cortex according to the position of the SPN in the striatum (Fig. 1F). Consistent with previous anatomical studies [3,9,41,42], we found that corticostriatal projections were topographically organized because SPNs located laterally in the dorsal striatum received synaptic inputs whose center of mass was in the lateral part of the barrel cortex (Fig. 1F,G; i.e., towards arcs of whisker columns with larger numbers essentially in this preparation; Supplemental Fig. 1A). This organization was not as precise as for the intracortical projections [43,44] because two cells in one given region of the dorsal striatum could receive input with centers of mass ~ 1 mm apart.

Individual SPNs have sparse input and specific innervation patterns

To evaluate the convergence of vibrissal inputs onto single SPNs, we describe clusters of innervation located on the horizontal axis of the LSPS grid of stimulation, which corresponds to the axis of barrels. Thus, clusters are defined hereafter as the ensemble of contiguous sites in the input map, collapsed along its vertical axis, where stimulation evoked EPSCs (Methods). SPNs received inputs from 1 to 6 clusters of cortical cells, 2 on average (Fig. 2A). The median width of the clusters was 150 µm (Fig. 2B), the width of a single barrel/column in this preparation (~ 100-200 µm). When confined to L5a, one median size cluster comprised one or few pyramidal cells as each was excited in a zone ~ 100 µm wide (Fig. 2B; Supplementals Fig.1 D). But the width of some clusters extended over several columns (Fig. 2B).

SPNs with a single cluster of inputs were occasionally found in the same slice and located nearby other SPNs with multiple clusters (Fig. 2C). This argued that for the former, the innervation from the portion of the barrel cortex present in the slice was genuinely low (i.e., not severed), like for the 35 % of SPNs that lacked any input in these slices. For SPNs with multiple clusters present in the slice, the fields of input, the spaces encompassing all their clusters, were large up to 1.6 mm, and thus hovered over multiple whisker cortical columns (Fig. 2D). However, their innervation was parcellated. Indeed clusters of cortical cells could be hundreds of micrometers apart and ~ 40 % of an input field collapsed along its vertical axis did not yield any synaptic response when stimulated (Fig. 2E). The amount of innervation did not increase proportionally with the width of the input field; in other words, the wider the field, the less dense the innervation (Fig. 2F). Finally, we observed a profound decrease, ~ -75 %, in the amplitude of the inputs provided by the adjacent clusters compared to the strongest cluster (Fig. 2G). This indicated that the SPN field of inputs was functionally sharp along the axis of barrels, even for SPNs innervated by multiple clusters of cells. Altogether, these data support the hypothesis of the discrete nature of innervation and sensory inputs associated with each SPN. It also reveals a great diversity in the spatial organization of clusters of cells in the barrel cortex that innervate the striatal cells, leading some SPNs to integrate a focal representation of cortical whisker columns and others to integrate a larger but parcellated representation of whisker columns.

The position of clusters, relative to each other in the input field, differed among SPNs. In particular, aligning all the input fields to the position of their strongest cluster did not allow the secondary clusters to be aligned (Fig. 2H). Thus, the projection to SPNs lacked a consistent organization relative to the arrangement of cortical columns. Within the same animal and slice, neurons shared little input as 60 % of all pairs had no overlap at all (median, 0 % of their inputs, Fig. 2I). However, input sharing was more common, 55 % of pairs, when SPNs were separated by 100 µm or less, horizontally (Fig. 2J, in red). These pairs shared 0 to 38 % of their inputs (median, 4 %). Again, this local organization was not stereotyped, as it was no longer seen when data from all animals were pooled (Fig. 2J, in black). These results suggest that the corticostriatal projection allowed SPNs located in close proximity (≤ 100 µm) to still share a small fraction of their cortical inputs, despite an overall low connectivity rate and the absence of a clearly defined innervation pattern.

Sensory projections to D1 and D2 SPNs are similar at the population level

Next, we investigated whether the organization of the projections from the barrel cortex was similar between neurons in the direct and indirect pathways. Based on previous studies on Drd1a-tdTomato mice, unlabeled ($D1^-$) SPNs were expressing the D2 type of dopamine receptors exclusively [45–49]. In addition, less than 5 % of all striatal neurons are local interneurons, indicating that the vast majority of unlabeled neurons in our experiments were $D2^+$ SPNs. As previously found [23], projections to D1 and D2 SPNs were spatially intermingled along the axis of barrels (i.e., medio-lateral axis; Fig. 3A; n = 47 and 54, cells respectively). The two subtypes received inputs from the same layers, in the same proportions (Fig. 3B). Finally, D1 and D2 SPNs received inputs with similar profiles as shown by their number of clusters and the sharpness of their input fields (Fig. 3C-G). However, D1/D2 differences were observed in the strength of projections, in a layer-specific manner. The sum of EPSCs ($EPSC^{\Sigma}$) evoked in every layer are compared here so as to make our results comparable to responses evoked with other stimulation methods. Whereas stimulations in L5a evoked similar $EPSC^{\Sigma}$ in D1 and D2 cells, differences were found in layers with a low incidence in the LSPS input maps. Indeed, L2/3-evoked $EPSC^{\Sigma}$ were stronger in D2 SPNs (91 ± 36 vs. 23 ± 22 pA, p = 0.005, Mann-Whitney) whereas L6-evoked $EPSC^{\Sigma}$ were stronger in D1 SPNs (37 ± 17 vs. 16 ± 2 pA, p = 0.0076). Altogether, these findings suggest that projections to D1 and D2 SPNs are globally similar, but that a dichotomy may be found in the properties of their less abundant cortical afferents.

Different patterns of innervation of the D1 and D2 SPNs correspond to different behavioral biases of the mice during thigmotaxis

Next, we tested the hypothesis that the patterns of innervation of the D1 and D2 SPNs are linked to the lateralization and speed of the mice's displacements guided by tactile input, two intrinsic behavioral biases. Hence, we analyzed the thigmotaxis of each mouse that had been placed in the dark within a large squared open field (OF) prior to the electrophysiological recordings (Fig. 4A). To evaluate the mouse eventual preference for tactile information contralateral to the investigated striatum (left hemisphere), we monitored the body side, left or right (LB and RB hereafter), the mouse exposed to the walls. As described previously [50], the mice's preference for tactile input from one side of the body was consistent when their lateralization was tested in two different settings (Supplemental Fig. 2A). Thus, the lateralization of thigmotaxis in the open field was an intrinsic bias of the mice. We also monitored the speed of the mice and the changes in speed-mode, high or low [51,52] (> or < 10 $cm.sec^{-1}$; Fig. 4A and supplemental Fig. 2C,D). As previously described [25,26], the speed at which mice moved along the walls of the OF was individual-specific and transferable to another environment (supplemental Fig. 2B).

The Spearman coefficients of the correlations between these behavioral parameters and key characteristics of the sensory projection to SPNs were computed to uncover associations and identify which property of innervations, strength or spatial organization, was involved. This revealed specific associations for the D1 and D2 subtypes, as indicated by the positions of the significant pairs that differed in the D1 and D2 matrices (green circles in Fig. 4B; $p < 0.0035$, 5 % false discovery rate or FDR). In addition, five of the tested pairs had a significantly different coefficient between D1 and D2 (+ symbols in Fig. 4B; $p < 0.0125$ taking the absolute values, 5 % FDR). Thus, the properties of the cortical projections targeting the two SPN subtypes appeared to be shaped in different manners, significantly more so than suggested by the population level analysis.

There was a positive relationship between the mouse propensity to switch to RB wall scanning and the number of clusters in the barrel cortex innervating D1 SPNs in the contralateral (left) hemisphere ($R = 0.47$, $p = 0.0021$, 5 % FDR, N = 35; Fig. 4C). There was no correlation when the reverse switch to LB wall scanning was considered ($R = 0.08$, $p > 0.05$) and it was degraded if the body side-changes were not detected reliably (i.e., if a large spatial binning of the OF was used; Supplemental Fig. 2H). These findings suggest that D1 SPNs received input from additional clusters in the hemisphere contralateral to the preferred tactile input. Consistent with this, D1 SPNs in the left hemisphere had significantly more clusters in mice that moved preferentially with their RB exposed to the walls than in other mice, 2 ± 0.3 vs. 1 ± 0.2 (Welch's t test, $p = 0.046$, Fig. 4D). Moreover, D1 SPNs without a single input in the slice were encountered 2 times less frequently in RB biased mice (23 % vs. 45 %; n = 31 and 40 recordings respectively; only slices with input are included; Fig. 4E). However, the width of the input fields was not significantly changed (263 ± 117 vs. 500 ± 106 µm, $p = 0.18$; Fig. 4F). Altogether, these results suggest an increased innervation of the input fields of D1 SPNs in mice that preferentially guide their displacements with the contralateral side of the body during the exploration of a novel environment (Fig. 4G).

The electrophysiology/behavior pairs showing a significant correlation in the D2 matrix linked the density of the input field of D2 SPNs with the mean speed of the mice in the high speed mode (RB side, $R = -0.63$, Spearman, $p < 0.001$, 5 % FDR; Fig. 4B,H) and with the probability that it switched to the high speed mode ($R = -0.53$, $p = 0.0035$, 5 % FDR, N = 34; Fig. 4I). The correlations were negative, as the least dense D2 SPNs input fields were observed in mice that travel the fastest (Fig. 4H). As described above, low density was a hallmark of the wide input fields (Fig. 2F). Indeed, D2 SPNs input fields greatly elongated in "fast mice'', by a factor of 5 from 110 ± 71 to 580 ± 71 µm ($p = 0.0042$, Mann-Whitney, ≤ vs > 18 $cm.s^{-1}$, the mice mean high speed on average; Fig. 4K). Thus, a critical factor of the variability of the

D2 SPN input fields was how broadly the innervating cortical cells were distributed along the axis of barrels. The density of the D2 SPN input field was also negatively correlated with the mean high speed of mice when they were exposing their other body side to walls, ipsilateral to the recording hemisphere (R = -0.50, p = 0.005; Fig. 4J). Testing different cut-offs for separating the two speed modes revealed that the density of D2 input fields reflected the mouse preference for a mode of displacement rather than a preference for mobility or immobility (Supplemental Fig. 2J). Taken together, these results suggest that in animals that tend to explore the OF slowly, D2 SPNs have a small input field in the barrel cortex (Fig. 4L). In contrast, in animals that tend to run, D2 SPNs have a large but parcellated input field in the barrel cortex.

Discussion

We investigated the organization of functional projections originating in the barrel cortex and targeting projection neurons in the dorsal striatum. We found that cortical neurons innervating one SPN were sparse, scattered in input fields wide up to 1.6 mm, separated by multiple whisker-columns, and principally located in L5a. This arrangement for a single sensory modality contrasts with the macroscopic organization of cortico-striatal projections, which is characterized by a higher degree of convergence. Here, each SPN had a distinct pattern of innervation from the barrel cortex, albeit with occasional overlaps for SPNs less than 100 µm apart. Patterns of innervation of SPNs were overall similar in the direct and indirect pathways. However this similarity was only apparent, and the sensory innervations of D1 and D2 SPNs were probably shaped according to different constraints, but in relation to the animal's spontaneous sensorimotor biases for both.

Sparse sensory innervation of single SPNs

As previously revealed by tracing of corticostriatal projections, the primary source of innervation of SPNs in this study is the upper part of L5 in the barrel cortex, L5a [23,37,53,54]. Also, SPNs are occasionally innervated by cells located in deeper and superficial layers [23,38,39,55]. Given the abundance of cortical axons in striatum, it has been assumed that a large number of cortical cells innervated each SPN, up to few thousands if synaptic connections were made promiscuously [56]. On the other hand, it has also been reported that neurons in the DLS fire in response to the stimulation of a single body-part in monkeys and rodents *in vivo*, even of a single whisker in some cases [11–13]. This finding suggests that each striatal neuron is in fact innervated by one small subregion of the somatosensory cortex. Consistent with these

findings, LSPS revealed here that neurons in the barrel cortex innervating a SPN are sparse, as shown by the number of clusters and the size of evoked EPSCs, averaging 2 and 40 pA respectively. 30 % of SPNs were innervated by a single whisker cortical column. Based on the small receptive fields of certain SPNs that were previously observed *in vivo* [11–13], it is possible that, intriguingly, for some of these SPNs the inputs detected by LSPS are the only inputs they have from the entire sensory cortex. Furthermore, even when a SPN was connected by several cortical clusters, a primary cluster could be identified, characterized by input strength substantially greater than that of the adjacent clusters. This pattern should also contribute to the sharpness of the receptive fields of SPNs. Altogether, our results suggest that, indeed, the integration of sensory information from the whisker pad, and perhaps other tactile organs, largely occurs at the population level of SPNs in the DLS, rather than at the level of individual cells. The sparse innervation is in striking contrast to the abundance of cortical axons in the DLS, suggesting that the sensory corticostriatal synapses are formed in a selective manner.

Specific cortical input to individual SPNs

A peculiar feature of the corticostriatal innervation is the disproportion between the number of cortical cells projecting to the striatum and the number of striatal cells, thought to be at a ratio of 10 to 1 [57]. Based on this ratio and the ultrastructure of the corticostriatal connection, C. Wilson's group concluded that the probability of an SPN being contacted by a given axon entering the domain of its dendritic arborization is low, 0.04 - 1.4 %, depending on the model. Hence, the chance that two SPNs are innervated by the same cortical axon is slim. Accordingly, we found here that the overlaps between LSPS input maps of different SPNs were scarce. In fact, nearby neurons could have input fields whose center of mass was 1 mm apart, indicating a loose topographic organization of the projection. This distance, 1 mm, corresponds to the width of cortical cell axonal arbor in the striatum [9,56]. Yet, LSPS maps of 2 SPNs had some overlap if the neurons were within 100 µm of each other, i.e., if their dendritic arbors overlapped. This was not predicted by the study of the ultrastructure of corticostriatal connections which posited, on the contrary, that two SPNs had a greater chance to be innervated by the same cortical cell if their dendrites deployed in different subregions of its axon arbor, as this would enhance the amount of available axonal boutons [56]. We attribute the difference to the fact that in our experiments neighboring SPNs were probably innervated by different neurons which were colocalized in the grid of stimulations positioned over the barrel cortex. This may indicate a mechanism by which neurons in close vicinity in cortex (< 100 µm) grow their axon in the exact same subregion of striatum (< 400 µm). Such a mechanism would permit the emergence of functional clusters in striatum as those described *in vivo* [11,13,58–60] and in brain slices [61]. In the future, dual recordings could test this hypothesis

specifically. It has already been shown that *in vivo*, nearby striatal cells responding to stimulation of the same part of the body still spiked with different latencies or showed different direction selectivities, consistent with the hypothesis of separate innervation even when originating from one small region in the cortex [11,13].

Similarities and specificities in the patterns of projection to SPNs in the direct and indirect pathways

How the inputs to D1 and D2 SPNs influence the differential effects of the direct and indirect pathways on basal ganglia outputs is unclear. Electrophysiological studies have shown that D1 SPNs exhibit larger responses than D2 SPNs to whisker deflections [15,20]. Also, the optostimulation of cortical efferents in brain slices showed a bias towards D1 SPNs [21,22]. In our study, we had contrasting results. Taking the projections globally, there was no difference in the innervation of D1 and D2 SPNs, neither in the rate at which cells were connected, nor in the organization of the projection. The principal layer innervating SPNs, L5a, delivered inputs of similar strengths to D1 and D2 SPNs. However, layers with lower incidence in the pattern of innervation showed bias in the amplitude of responses: Stimulations in L2/3 induced stronger responses in D2 cells whereas stimulations in L6 activated D1 cells more strongly. We have shown that stimulation in L2/3 activates true L2/3 projection. Similarly, L6-evoked EPSCs could indicate rare L6 projections to striatum, as these were previously described [38,39]. However, it is also possible that LSPS at the top of L6 effectively stimulated the proximal dendrites of neurons whose soma was located at the bottom of L5B. Our results would be consistent with the previous findings that D1 SPNs are more strongly innervated than D2 SPNs by cortical projection neurons of the pyramidal tract [22], as these are proportionally more present in deep layer 5 [62]. The larger L2/3 inputs received by the D2 SPNs is intriguing because of the role of this layer in higher-order integration processes, such as those activated during operand sensory discrimination tasks [63–65]. Moreover, L2/3 cells activity during the mouse displacement is distinctive, with a sustained response to ongoing wall touch as opposed to the transient response observed in L5 [66]. Further investigation is needed to specifically examine projections from the upper and lower cortical layers and how they influence the dynamics of sensory integration in the direct and indirect pathways of the DLS. However, these data illustrate the diversity of paths of sensory integration involving D1 and D2 SPNs.

D1 and D2 patterns of innervation associated with the animal's behavioral biases as they spontaneously sample tactile input from a novel environment

It is well known that unilateral alterations in striatum provoke lateralized behaviors in rodents [67]. The motor imbalance, that causes the rotation of the animal on itself, has received a lot of attention. However, it should not be confused with the sensory asymmetry studied here, which was revealed by the presence of walls to which mice were attracted during spontaneous exploration [68]. As previously reported [69], there were as many right and left "whiskered" mice in this study. The origin of this intrinsic lateralization is thought to reside in left/right asymmetries of the dopaminergic system and other signaling molecules in striatum [67,70], but a lateralized activity was also reported in the barrel cortex upon bilateral whisker stimulation [71]. To our knowledge, we provide the first evidence that different levels of sensory innervation to the striatum are associated with the preferential use of the contralateral side by mice for sampling tactile input. The fact that the number of clusters was increased suggests that this stronger innervation allowed the D1 SPNs to be connected by more cortical columns. Interestingly, this occurred in the absence of a significant increase in the width of their input fields, suggesting that the "additional" clusters primarily consolidated the D1 SPN input fields. The variability in the number of clusters per D1 SPN observed in the mice with a preference for RB inputs was large, with some cells still receiving inputs from a single cluster in the slice (Fig. 4D). It is possible that these SPNs had more clusters located along the antero-posterior axis of the brain, i.e., in other slices. In other words, the number of clusters innervating D1 SPNs may have increased both in the arc and row axis of the whisker columns of the barrel cortex. Alternatively, the densification of the input fields may only affect a fraction of the D1 SPNs.

The patterns of innervation of D2 SPNs did not correlate with the lateralization of mice. Instead, we found that the density of the D2 SPN input field was negatively correlated with the speed of the mice in the OF, which we could attribute to differences affecting the width of the input fields. Thus, D2 SPN input fields in fast mice were particularly wide in the axis of the barrel arcs present in the slice, although they were still parcellated. SPNs are active during spontaneous locomotion [30,58] , but it is still unclear how this activity is generated. Our results raise the hypothesis that the functions of D2 SPNs are well supported by circuits in which these cells have large input fields in the barrel cortex, with multiple and distant arcs of whisker columns. On the rodent snout, arcs of whiskers are arranged on the rostro-caudal axis, which coincides with the axis of mouse displacements. The observation that the D2 correlation with speed did not depend on the side of the body exposed to the wall suggests that the relevant tactile stimuli were not caused by contacts with the wall, but with the floor [31]. Thus, large input fields in the

axis of barrel arcs may not only allow for more convergence but also for different temporal dynamics in the integration of tactile inputs during motion. In fact, it has been shown that stimulation moving across the whisker pad evokes complex neuronal responses in the barrel cortex that may encode spatial information [72,73]. Furthermore, in addition to scanning surfaces, some whiskers and the activity of their corresponding cortical neurons are also speed detectors [31]. Thus, the activity of the vibrissal corticostriatal projection to SPNs may encode the ego-velocity of the animal. From this perspective, the correlation found for D2 SPN innervation patterns suggests that mice adapt their speed to their real-time processing capacity.

In conclusion, we found that the vibrissal sensory innervation of each SPN is sparse and specific, which, given the abundance of cortical axons in the DLS, argues that the formation of sensory corticostriatal synapses is selective. Sensory integration necessarily occurs at the population level because individual SPNs only have a limited representation of the whisker columns. Altogether, our results suggest that the sensory cortical wiring in the striatum offers great functional flexibility to SPNs, enabling their input to align with the tactile sampling behavior of mice.

Materials and Methods

Animals and ethics

Hemizygous male and female B6.Cg-Tg(Drd1a-tdTomato)6Calak/J mice (postnatal day [PND] 22–43) were used in accordance with institutional guidelines and the French Ministry of Research (APAFIS#27242). Mice were ear punched for identification. Mice were housed at constant room temperature (21° C) and humidity (60 %) and exposed to a reverse light cycle of 12 h light/dark with food and water available ad libitum.

Brain slices preparation and electrophysiology.

Mice were deeply anesthetized with isoflurane (4 %) prior to cervical dislocation and decapitation. We prepared corticostriatal slices (350 µm thick) from the brain left hemisphere, based on stereotaxic coordinates placing the striatal cells 1-2 mm anteriorly to the projection neurons in the barrel cortex [17,18]. Parasagittal slices were cut with a 60° angle from the midline and a 10° angle in the dorso-ventral axis (supplemental Fig. 1A) in a chilled cutting solution containing (in mM): 110 choline chloride, 25 NaHCO3, 25 D-glucose, 11.6 sodium ascorbate, 7 MgCl2, 3.1 sodium pyruvate, 2.5 KCl, 1.25 NaH2PO4, and 0.5 CaCl2 (Sigma Aldrich). Slices were then transferred to artificial cerebrospinal fluid (ACSF)

containing (in mM): 127 NaCl, 25 NaHCO3, 25 D-glucose, 2.5 KCl, 1 MgCl2, 2 CaCl2, and 1.25 NaH2PO4, aerated with 95% O2/5% CO2. Slices were first incubated at 34 °C for 30 min and then maintained at room temperature for 20 min prior to use. Slices used for LSPS contained barrels in the L4 of cortex, the globus pallidus, its external segment (GPe), the internal capsule, the ventral posteromedial nucleus of thalamus and the anterior hippocampus. 5 to 13 barrels were visible in the slice. 2 rows of barrels may be superimposed, explaining the largest numbers of barrels (supplemental Fig. 1A). SPNs 50–150 µm deep in the slice were visualized under infrared and fluorescent lights in a BX61WI microscope (Olympus) and patched with borosilicate electrodes (3–6 MΩ) and recorded in the voltage-clamp whole-cell configuration using a Multiclamp 700A amplifier (Axon Instrument, Molecular Devices). The holding membrane potential was – 80 mV. The intracellular solution contained (in mM) 128 Cs-methylsulfate, 4 MgCl2, 10 HEPES, 1 EGTA, 4 Na2ATP, 0.4 Na2GTP, 10 Na-phosphocreatine, 3 ascorbic acid; pH 7.25; 290-300 mOsm. Cells in L5 and L2/3 of the barrel cortex were recorded in the current-clamp mode, with an intracellular solution in which Cs-methylsulfate was replaced by K-methylsulfate. All experiments were performed at room temperature (21°C).

LSPS with glutamate uncaging

LSPS was performed as described previously [19]. Recirculating (2 mL/min) ACSF solution contained (in mM): 0.2 MNI-caged glutamate (Tocris), 0.005 CPP [()-3-(2-carboxypiperazin-4-yl) propyl-1-phosphonic acid], 4 $CaCl_2$, and 4 $MgCl_2$. Focal photolysis of caged glutamate was accomplished with a 2 ms 20mW pulse of a pulsed UV (355 nm) laser (DPSS Lasers Inc.) through a 0.16 NA 4 × objective (Olympus). 25 mW laser pulses were used for stimulating cortical neurons in mice older than P30 to maintain their excitation at a similar level than in younger mice (Supplemental Fig. 1C). The stimulus pattern for mapping the corticostriatal projections was 464 positions spaced by 75 µm on a 29 × 16 grid (2.1 × 1.1 mm) over barrel cortex. The corticostriatal slice and the LSPS grid were oriented in such a way that layer 5a was laid out horizontally. UV stimuli were applied every 700 ms and their successive positions on the LSPS grid was such as to maximize the time between stimulations of neighboring sites. Electrophysiological traces consisted of 100 ms baseline, a 450 ms window followed by a -5 mV / 100 ms test pulse. A minimum of 2 and up to 4 stimulations were performed at each site at several minutes intervals. Custom software for instrument control and acquisition [74] was written in Matlab (Mathworks). At the end of each experiment, a picture of the slice was saved in order to superpose it digitally to other slices, according to visual landmarks, with Adobe Photoshop (Adobe Inc.). Excitation profiles of pyramidal neurons were generated under similar conditions except that cells were recorded in current-clamp mode and glutamate was uncaged on a smaller 8 × 8 grid covering their soma and dendrites (50

μm spacing; 350 × 350 μm; Supplemental Fig. 1B). In a subset of L5a cell recordings, a 8 × 24 grid was used to stimulate up in L1 (50 μm spacing; Supplemental Fig. 1B).

Analysis of LSPS data

Synaptic input maps of neurons were constructed by taking the peak amplitude of EPSCs detected in a 50 ms time window starting at stimulation onset for each position in the LSPS grid. Measures were averaged across repetitions of stimulations (2-4). The threshold for EPSC detection was 3 standard deviations from baseline, or 9.2 ± 0.4 pA. To disambiguate evoked responses from spontaneous activity, synaptic responses occurring less than 2 times across repetitions of maps were set to zero. Averaged maps were superposed taking L5a as reference in the vertical axis and the junction of the GPe, dorsal striatum and internal capsule as reference in the horizontal axis (Ref_{hor}). In order to detect clusters and the center of mass of inputs in the LSPS map, we used the binary version of the map reporting the location of connected and non-connected sites (i.e., yielding EPSCs or none in the recorded SPN) and stacked it along its vertical axis. A cluster of inputs comprised 1 or more consecutive connected sites in the stacked map that was framed by 1 or more non-connected sites. Thus, a cluster here may include connected sites that were not adjacent on the vertical axis in the original map, and may combine synaptic inputs from different layers. The input center of mass in the horizontal axis was computed as : Σ (connected sites × lateral distances from Ref_{hor})/Σ (connected sites). Traces from current clamp recordings were analyzed in a 50 ms time window at stimulus onset to count the number of action potentials (APs) elicited upon glutamate uncaging at every site and in the entire stimulation grid. Non parametric statistical tests were used. Everywhere n is the number of cells and N the number of mice.

Spontaneous locomotion behavior

Prior to electrophysiology experiments, mice were placed in an open field (OF; 70 x 80 cm) inside a wooden chamber illuminated with red LEDs. The position of their body center of mass was tracked during 20 min at 20 Hz by a DMK 23UMO21 camera (Imaging Source) and Labview (National Instruments) and their displacements were analyzed in Matlab. In the analysis, the border of the OF was divided in 20 zones (11 cm) [75,76] and the side of the body that mice exposed to the walls, left or right (LB and RB), their speed, and speed-mode (low, < 10 $cm.sec^{-1}$; high, ≥ 10 $cm.sec^{-1}$) [51,52] were analyzed at each visit of a zone. Speed was the distance traveled inside a zone divided by the time spent in that zone. This allowed computing probabilities (p.) of changing body side or speed mode during thigmotaxis [74]. Precisely, the monitored parameters were: *P. switch to fast mode, RB* is p. of switching from the low to the high speed mode, during RB thigmotactic scanning; *Mean high speed, RB* is averaged speed in

zones where mice were in high speed mode, during RB thigmotactic scanning; *P. turn to RB scan* is p. of switching from LB to RB thigmotactic scanning; *P. RB scan* is p. of thigmotactic scanning with the RB.

Electrophysiology/Behavior correlation matrices

A correlation matrix was assembled from the Spearman correlation coefficients of 20 electrophysiology/behavior pairs for D1 SPNs and D2 SPNs. The electrophysiological parameters of each cell were: *Input field width* is the horizontal length in cortex containing all sites that evoked an EPSC; *Clusters* is number of clusters; $Clust_I$ *input* is the sum of EPSCs evoked by stimulation in the strongest cluster; *Connected sites* is the total number of sites where stimulation evoked an EPSC; *Input field density* is the [connected sites / input field width] ratio. Electrophysiological parameters were averaged if more than one SPN of the same pathway (D1 or D2) were obtained per animal. This concerned 10 out of 35 mice for the D1 SPN data set and 14 out of 34 mice for the D2 SPN data set (2 to 3 cells per mice). Variables were ordered according to hierarchical clustering in the correlation matrices (Ward's linkage method, Supplemental Fig. 2F).

To detect pairs of electrophysiological/behavioral variables in the D1 or D2 matrix of correlations that were statistically significant, 3000 surrogates were generated by associating each set (i.e., from one mouse) of electrophysiological data with a set of behavioral data picked randomly from the pool of D1 or D2 data, without replacement. The Spearman correlation coefficient (R, Fisher transformed) of an electrophysiology/behavior pair was considered significant if it was outside the 95 % confidence interval of the R of surrogate pairs. False discovery rates (FDR) were computed for each electrophysiology/behavior pair according to the procedure of Benjamini-Hochberg for multiple testing. For testing the differences between the absolute values of the correlation coefficients of D1 and D2 pairs ($\Delta|R| = |R|_{D1}-|R|_{D2}$); R Fisher transformed), surrogate pairs were made from the random pick of electrophysiological and behavioral data set, half from the D1 data, the other half from the D2 data, with replacement. We tested whether the actual $\Delta|R|$ was outside the 95 % confidence interval of the $\Delta|R|$ of surrogate pairs. The FDR were computed according to the procedure of Benjamini-Hochberg.

Acknowledgments

This work was supported by funding from the Institut National de la Santé et de la Recherche Médicale and a grant from the Agence Nationale de la Recherche (Corticostriatal, ANR-20-CE16-0002). K. Amroune is supported by fellowships from the Ministère de l'Enseignement Supérieur et de la Recherche and from the French government under the "France 2030" program via A*Midex (Initiative d'Excellence d'Aix-Marseille Université, AMX-19-IET-004) and ANR funding (ANR-17-EURE-0029). L. Fontolan is supported by funding from Excellence Initiative of Aix Marseille Université - A*MIDEX (Turing Centre for Living Systems). We thank the staff at the animal and genotyping facilities of INMED, and the members of the CBGB group for their help and support. We thank Elodie Fino, Rosa Cossart, Ede Rancz and Roustem Khazipov for their critical reading of the manuscript.

References

1. Nelson, A.B., and Kreitzer, A.C. (2014). Reassessing models of basal ganglia function and dysfunction. Annu. Rev. Neurosci. *37*, 117–135. 10.1146/annurev-neuro-071013-013916.
2. Robbe, D. (2018). To move or to sense? Incorporating somatosensory representation into striatal functions. Curr. Opin. Neurobiol. *52*, 123–130. 10.1016/j.conb.2018.04.009.
3. Flaherty, A.W., and Graybiel, A.M. (1991). Corticostriatal transformations in the primate somatosensory system. Projections from physiologically mapped body-part representations. J. Neurophysiol. *66*, 1249–1263. 10.1152/jn.1991.66.4.1249.
4. Flaherty, A.W., and Graybiel, A.M. (1994). Input-output organization of the sensorimotor striatum in the squirrel monkey. J. Neurosci. Off. J. Soc. Neurosci. *14*, 599–610. 10.1523/JNEUROSCI.14-02-00599.1994.
5. Alloway, K.D., Mutic, J.J., Hoffer, Z.S., and Hoover, J.E. (2000). Overlapping corticostriatal projections from the rodent vibrissal representations in primary and secondary somatosensory cortex. J. Comp. Neurol. *428*, 51–67.
6. Smith, J.B., Chakrabarti, S., Mowery, T.M., and Alloway, K.D. (2022). Convergence of forepaw somatosensory and motor cortical projections in the striatum, claustrum, thalamus, and pontine nuclei of cats. Brain Struct. Funct. *227*, 361–379. 10.1007/s00429-021-02405-6.
7. Hintiryan, H., Foster, N.N., Bowman, I., Bay, M., Song, M.Y., Gou, L., Yamashita, S., Bienkowski, M.S., Zingg, B., Zhu, M., et al. (2016). The mouse cortico-striatal projectome. Nat. Neurosci. *19*, 1100–1114. 10.1038/nn.4332.
8. Hunnicutt, B.J., Jongbloets, B.C., Birdsong, W.T., Gertz, K.J., Zhong, H., and Mao, T. (2016). A comprehensive excitatory input map of the striatum reveals novel functional organization. eLife *5*, e19103. 10.7554/eLife.19103.
9. Hooks, B.M., Papale, A.E., Paletzki, R.F., Feroze, M.W., Eastwood, B.S., Couey, J.J., Winnubst, J., Chandrashekar, J., and Gerfen, C.R. (2018). Topographic precision in sensory and motor corticostriatal projections varies across cell type and cortical area. Nat. Commun. *9*, 3549. 10.1038/s41467-018-05780-7.
10. Sanabria, B.D., Baskar, S.S., Yonk, A.J., Linares-Garcia, I., Abraira, V.E., Lee, C.R., and Margolis, D.J. (2024). Cell-Type Specific Connectivity of Whisker-Related Sensory and Motor Cortical Input to

Dorsal Striatum. eneuro *11*, ENEURO.0503-23.2023. 10.1523/ENEURO.0503-23.2023.
11. Carelli, R.M., and West, M.O. (1991). Representation of the body by single neurons in the dorsolateral striatum of the awake, unrestrained rat. J. Comp. Neurol. *309*, 231–249. 10.1002/cne.903090205.
12. Cho, J., and West, M.O. (1997). Distributions of single neurons related to body parts in the lateral striatum of the rat. Brain Res. *756*, 241–246. 10.1016/s0006-8993(97)00143-1.
13. Jaeger, D., Gilman, S., and Aldridge, J.W. (1995). Neuronal activity in the striatum and pallidum of primates related to the execution of externally cued reaching movements. Brain Res. *694*, 111–127. 10.1016/0006-8993(95)00780-t.
14. Charpier, S., Pidoux, M., and Mahon, S. (2020). Converging sensory and motor cortical inputs onto the same striatal neurons: An in vivo intracellular investigation. PLOS ONE *15*, e0228260. 10.1371/journal.pone.0228260.
15. Reig, R., and Silberberg, G. (2014). Multisensory integration in the mouse striatum. Neuron *83*, 1200–1212. 10.1016/j.neuron.2014.07.033.
16. Schmidt, S.L., Filgueiras, C.C., and Krahe, T.E. (1999). Effects of sex and laterality on the rotatory swimming behavior of normal mice. Physiol. Behav. *65*, 607–616. 10.1016/s0031-9384(98)00184-x.
17. Aronoff, R., Matyas, F., Mateo, C., Ciron, C., Schneider, B., and Petersen, C.C.H. (2010). Long-range connectivity of mouse primary somatosensory barrel cortex. Eur. J. Neurosci. *31*, 2221–2233. 10.1111/j.1460-9568.2010.07264.x.
18. de la Torre-Martinez, R., Ketzef, M., and Silberberg, G. (2023). Ongoing movement controls sensory integration in the dorsolateral striatum. Nat. Commun. *14*, 1004. 10.1038/s41467-023-36648-0.
19. Bureau, I., von Saint Paul, F., and Svoboda, K. (2006). Interdigitated paralemniscal and lemniscal pathways in the mouse barrel cortex. PLoS Biol. *4*, e382. 10.1371/journal.pbio.0040382.
20. Filipović, M., Ketzef, M., Reig, R., Aertsen, A., Silberberg, G., and Kumar, A. (2019). Direct pathway neurons in mouse dorsolateral striatum in vivo receive stronger synaptic input than indirect pathway neurons. J. Neurophysiol. *122*, 2294–2303. 10.1152/jn.00481.2019.
21. Parker, P.R.L., Lalive, A.L., and Kreitzer, A.C. (2016). Pathway-Specific Remodeling of Thalamostriatal Synapses in Parkinsonian Mice. Neuron *89*, 734–740. 10.1016/j.neuron.2015.12.038.
22. Kress, G.J., Yamawaki, N., Wokosin, D.L., Wickersham, I.R., Shepherd, G.M.G., and Surmeier, D.J. (2013). Convergent cortical innervation of striatal projection neurons. Nat. Neurosci. *16*, 665–667. 10.1038/nn.3397.
23. Wall, N.R., De La Parra, M., Callaway, E.M., and Kreitzer, A.C. (2013). Differential innervation of direct- and indirect-pathway striatal projection neurons. Neuron *79*, 347–360. 10.1016/j.neuron.2013.05.014.
24. Schwarting, R.K., Steiner, H., and Huston, J.P. (1991). Asymmetries in thigmotactic scanning: evidence for a role of dopaminergic mechanisms. Psychopharmacology (Berl.) *103*, 19–27. 10.1007/BF02244068.
25. Lewejohann, L., Zipser, B., and Sachser, N. (2011). “Personality” in laboratory mice used for biomedical research: a way of understanding variability? Dev. Psychobiol. *53*, 624–630. 10.1002/dev.20553.
26. Friedman, W.A., Garland, T., and Dohm, M.R. (1992). Individual variation in locomotor behavior and maximal oxygen consumption in mice. Physiol. Behav. *52*, 97–104. 10.1016/0031-9384(92)90438-8.
27. Luhmann, H.J., Huston, J.P., and Hasenöhrl, R.U. (2005). Contralateral increase in thigmotactic scanning following unilateral barrel-cortex lesion in mice. Behav. Brain Res. *157*, 39–43. 10.1016/j.bbr.2004.06.006.
28. Schwarting, R.K., Goldenberg, R., Steiner, H., Fornaguera, J., and Huston, J.P. (1993). A video image analyzing system for open-field behavior in the rat focusing on behavioral asymmetries. J. Neurosci. Methods *49*, 199–210. 10.1016/0165-0270(93)90125-b.

29. Ljungberg, T., and Ungerstedt, U. (1976). Sensory inattention produced by 6-hydroxydopamine-induced degeneration of ascending dopamine neurons in the brain. Exp. Neurol. *53*, 585–600. 10.1016/0014-4886(76)90140-0.
30. Tecuapetla, F., Matias, S., Dugue, G.P., Mainen, Z.F., and Costa, R.M. (2014). Balanced activity in basal ganglia projection pathways is critical for contraversive movements. Nat. Commun. *5*, 4315. 10.1038/ncomms5315.
31. Chorev, E., Preston-Ferrer, P., and Brecht, M. (2016). Representation of egomotion in rat's trident and E-row whisker cortices. Nat. Neurosci. *19*, 1367–1373. 10.1038/nn.4363.
32. Yttri, E.A., and Dudman, J.T. (2016). Opponent and bidirectional control of movement velocity in the basal ganglia. Nature *533*, 402–406. 10.1038/nature17639.
33. Freeze, B.S., Kravitz, A.V., Hammack, N., Berke, J.D., and Kreitzer, A.C. (2013). Control of basal ganglia output by direct and indirect pathway projection neurons. J. Neurosci. Off. J. Soc. Neurosci. *33*, 18531–18539. 10.1523/JNEUROSCI.1278-13.2013.
34. Shepherd, G.M.G., Pologruto, T.A., and Svoboda, K. (2003). Circuit analysis of experience-dependent plasticity in the developing rat barrel cortex. Neuron *38*, 277–289. 10.1016/s0896-6273(03)00152-1.
35. Bureau, I., Shepherd, G.M.G., and Svoboda, K. (2008). Circuit and plasticity defects in the developing somatosensory cortex of FMR1 knock-out mice. J. Neurosci. Off. J. Soc. Neurosci. *28*, 5178–5188. 10.1523/JNEUROSCI.1076-08.2008.
36. Cowan, R.L., and Wilson, C.J. (1994). Spontaneous firing patterns and axonal projections of single corticostriatal neurons in the rat medial agranular cortex. J. Neurophysiol. *71*, 17–32. 10.1152/jn.1994.71.1.17.
37. Wise, S.P., and Jones, E.G. (1977). Cells of origin and terminal distribution of descending projections of the rat somatic sensory cortex. J. Comp. Neurol. *175*, 129–157. 10.1002/cne.901750202.
38. Guo, C., Peng, J., Zhang, Y., Li, A., Li, Y., Yuan, J., Xu, X., Ren, M., Gong, H., and Chen, S. (2017). Single-axon level morphological analysis of corticofugal projection neurons in mouse barrel field. Sci. Rep. *7*, 2846. 10.1038/s41598-017-03000-8.
39. Bertero, A., Verrillo, L., and Apicella, A.J. (2022). A Novel Layer 4 Corticofugal Cell Type/Projection Involved in Thalamo-Cortico-Striatal Sensory Processing. J. Neurosci. Off. J. Soc. Neurosci. *42*, 1383–1405. 10.1523/JNEUROSCI.1738-21.2021.
40. Morita, K., Im, S., and Kawaguchi, Y. (2019). Differential Striatal Axonal Arborizations of the Intratelencephalic and Pyramidal-Tract Neurons: Analysis of the Data in the MouseLight Database. Front. Neural Circuits *13*, 71. 10.3389/fncir.2019.00071.
41. Alloway, K.D., Crist, J., Mutic, J.J., and Roy, S.A. (1999). Corticostriatal projections from rat barrel cortex have an anisotropic organization that correlates with vibrissal whisking behavior. J. Neurosci. Off. J. Soc. Neurosci. *19*, 10908–10922. 10.1523/JNEUROSCI.19-24-10908.1999.
42. Wright, A.K., Norrie, L., Ingham, C.A., Hutton, E.A., and Arbuthnott, G.W. (1999). Double anterograde tracing of outputs from adjacent "barrel columns" of rat somatosensory cortex. Neostriatal projection patterns and terminal ultrastructure. Neuroscience *88*, 119–133. 10.1016/s0306-4522(98)00186-9.
43. Shepherd, G.M.G., and Svoboda, K. (2005). Laminar and columnar organization of ascending excitatory projections to layer 2/3 pyramidal neurons in rat barrel cortex. J. Neurosci. Off. J. Soc. Neurosci. *25*, 5670–5679. 10.1523/JNEUROSCI.1173-05.2005.
44. Erlandson, M.A., Manzoni, O.J., and Bureau, I. (2015). The Functional Organization of Neocortical Networks Investigated in Slices with Local Field Recordings and Laser Scanning Photostimulation. PloS One *10*, e0132008. 10.1371/journal.pone.0132008.
45. Bertran-Gonzalez, J., Bosch, C., Maroteaux, M., Matamales, M., Hervé, D., Valjent, E., and Girault, J.-A. (2008). Opposing patterns of signaling activation in dopamine D1 and D2 receptor-expressing striatal neurons in response to cocaine and haloperidol. J. Neurosci. Off. J. Soc. Neurosci. *28*, 5671–

5685. 10.1523/JNEUROSCI.1039-08.2008.
46. Ade, K.K., Wan, Y., Chen, M., Gloss, B., and Calakos, N. (2011). An Improved BAC Transgenic Fluorescent Reporter Line for Sensitive and Specific Identification of Striatonigral Medium Spiny Neurons. Front. Syst. Neurosci. *5*, 32. 10.3389/fnsys.2011.00032.
47. Enoksson, T., Bertran-Gonzalez, J., and Christie, M.J. (2012). Nucleus accumbens D2- and D1-receptor expressing medium spiny neurons are selectively activated by morphine withdrawal and acute morphine, respectively. Neuropharmacology *62*, 2463–2471. 10.1016/j.neuropharm.2012.02.020.
48. Thibault, D., Loustalot, F., Fortin, G.M., Bourque, M.-J., and Trudeau, L.-É. (2013). Evaluation of D1 and D2 Dopamine Receptor Segregation in the Developing Striatum Using BAC Transgenic Mice. PLoS ONE *8*, e67219. 10.1371/journal.pone.0067219.
49. Cao, J., Dorris, D.M., and Meitzen, J. (2018). Electrophysiological properties of medium spiny neurons in the nucleus accumbens core of prepubertal male and female Drd1a-tdTomato line 6 BAC transgenic mice. J. Neurophysiol. *120*, 1712–1727. 10.1152/jn.00257.2018.
50. Aggestam, F., and Cahusac, P.M.B. (2007). Behavioural lateralization of tactile performance in the rat. Physiol. Behav. *91*, 335–339. 10.1016/j.physbeh.2007.03.015.
51. Granon, S., Faure, P., and Changeux, J.-P. (2003). Executive and social behaviors under nicotinic receptor regulation. Proc. Natl. Acad. Sci. U. S. A. *100*, 9596–9601. 10.1073/pnas.1533498100.
52. Sheets, A.L., Lai, P.-L., Fisher, L.C., and Basso, D.M. (2013). Quantitative evaluation of 3D mouse behaviors and motor function in the open-field after spinal cord injury using markerless motion tracking. PloS One *8*, e74536. 10.1371/journal.pone.0074536.
53. Reiner, A., Jiao, Y., Del Mar, N., Laverghetta, A.V., and Lei, W.L. (2003). Differential morphology of pyramidal tract-type and intratelencephalically projecting-type corticostriatal neurons and their intrastriatal terminals in rats. J. Comp. Neurol. *457*, 420–440. 10.1002/cne.10541.
54. Shepherd, G.M.G. (2013). Corticostriatal connectivity and its role in disease. Nat. Rev. Neurosci. *14*, 278–291. 10.1038/nrn3469.
55. Yamashita, T., Vavladeli, A., Pala, A., Galan, K., Crochet, S., Petersen, S.S.A., and Petersen, C.C.H. (2018). Diverse Long-Range Axonal Projections of Excitatory Layer 2/3 Neurons in Mouse Barrel Cortex. Front. Neuroanat. *12*, 33. 10.3389/fnana.2018.00033.
56. Anthony E. Kincaid, Tong Zheng, and Charles J. Wilson (1998). Connectivity and Convergence of Single Corticostriatal Axons. J. Neurosci. *18*, 4722. 10.1523/JNEUROSCI.18-12-04722.1998.
57. Oorschot, D.E. (1996). Total number of neurons in the neostriatal, pallidal, subthalamic, and substantia nigral nuclei of the rat basal ganglia: a stereological study using the cavalieri and optical disector methods. J. Comp. Neurol. *366*, 580–599. 10.1002/(SICI)1096-9861(19960318)366:4<580::AID-CNE3>3.0.CO;2-0.
58. Barbera, G., Liang, B., Zhang, L., Gerfen, C.R., Culurciello, E., Chen, R., Li, Y., and Lin, D.-T. (2016). Spatially Compact Neural Clusters in the Dorsal Striatum Encode Locomotion Relevant Information. Neuron *92*, 202–213. 10.1016/j.neuron.2016.08.037.
59. Klaus, A., Martins, G.J., Paixao, V.B., Zhou, P., Paninski, L., and Costa, R.M. (2017). The Spatiotemporal Organization of the Striatum Encodes Action Space. Neuron *95*, 1171-1180.e7. 10.1016/j.neuron.2017.08.015.
60. Weglage, M., Wärnberg, E., Lazaridis, I., Calvigioni, D., Tzortzi, O., and Meletis, K. (2021). Complete representation of action space and value in all dorsal striatal pathways. Cell Rep. *36*, 109437. 10.1016/j.celrep.2021.109437.
61. Badreddine, N., Zalcman, G., Appaix, F., Becq, G., Tremblay, N., Saudou, F., Achard, S., and Fino, E. (2022). Spatiotemporal reorganization of corticostriatal networks encodes motor skill learning. Cell Rep. *39*, 110623. 10.1016/j.celrep.2022.110623.
62. Ramaswamy, S., and Markram, H. (2015). Anatomy and physiology of the thick-tufted layer 5

pyramidal neuron. Front. Cell. Neurosci. *9*. 10.3389/fncel.2015.00233.
63. Han, S., and Helmchen, F. (2024). Behavior-relevant top-down cross-modal predictions in mouse neocortex. Nat. Neurosci. *27*, 298–308. 10.1038/s41593-023-01534-x.
64. Kwon, S.E., Yang, H., Minamisawa, G., and O'Connor, D.H. (2016). Sensory and decision-related activity propagate in a cortical feedback loop during touch perception. Nat. Neurosci. *19*, 1243–1249. 10.1038/nn.4356.
65. Oryshchuk, A., Sourmpis, C., Weverbergh, J., Asri, R., Esmaeili, V., Modirshanechi, A., Gerstner, W., Petersen, C.C.H., and Crochet, S. (2024). Distributed and specific encoding of sensory, motor, and decision information in the mouse neocortex during goal-directed behavior. Cell Rep. *43*, 113618. 10.1016/j.celrep.2023.113618.
66. Ayaz, A., Stäuble, A., Hamada, M., Wulf, M.-A., Saleem, A.B., and Helmchen, F. (2019). Layer-specific integration of locomotion and sensory information in mouse barrel cortex. Nat. Commun. *10*, 2585. 10.1038/s41467-019-10564-8.
67. Molochnikov, I., and Cohen, D. (2014). Hemispheric differences in the mesostriatal dopaminergic system. Front. Syst. Neurosci. *8*. 10.3389/fnsys.2014.00110.
68. Sullivan, R.M., Fraser, A., and Szechtman, H. (1994). Asymmetrical orientation to edges of an openfield: modulation by striatal dopamine and relationship to motor asymmetries in the rat. Brain Res. *637*, 114–118. 10.1016/0006-8993(94)91223-8.
69. Morice, E., Denis, C., Macario, A., Giros, B., and Nosten-Bertrand, M. (2005). Constitutive Hyperdopaminergia is Functionally Associated with Reduced Behavioral Lateralization. Neuropsychopharmacology *30*, 575–581. 10.1038/sj.npp.1300570.
70. Grabrucker, S., Haderspeck, J.C., Sauer, A.K., Kittelberger, N., Asoglu, H., Abaei, A., Rasche, V., Schön, M., Boeckers, T.M., and Grabrucker, A.M. (2017). Brain Lateralization in Mice Is Associated with Zinc Signaling and Altered in Prenatal Zinc Deficient Mice That Display Features of Autism Spectrum Disorder. Front. Mol. Neurosci. *10*, 450. 10.3389/fnmol.2017.00450.
71. de Celis Alonso, B., Sergeyeva, M., Brune, K., and Hess, A. (2012). Lateralization of responses to vibrissal stimulation: connectivity and information integration in the rat sensory-motor cortex assessed with fMRI. NeuroImage *62*, 2101–2109. 10.1016/j.neuroimage.2012.05.045.
72. Benison, A.M., Ard, T.D., Crosby, A.M., and Barth, D.S. (2006). Temporal patterns of field potentials in vibrissa/barrel cortex reveal stimulus orientation and shape. J. Neurophysiol. *95*, 2242–2251. 10.1152/jn.01034.2005.
73. Ego-Stengel, V., Mello e Souza, T., Jacob, V., and Shulz, D.E. (2005). Spatiotemporal characteristics of neuronal sensory integration in the barrel cortex of the rat. J. Neurophysiol. *93*, 1450–1467. 10.1152/jn.00912.2004.
74. Suter, B.A., O'Connor, T., Iyer, V., Petreanu, L.T., Hooks, B.M., Kiritani, T., Svoboda, K., and Shepherd, G.M.G. (2010). Ephus: multipurpose data acquisition software for neuroscience experiments. Front. Neural Circuits *4*, 100. 10.3389/fncir.2010.00100.
75. Tanaka, S., Young, J.W., Halberstadt, A.L., Masten, V.L., and Geyer, M.A. (2012). Four factors underlying mouse behavior in an open field. Behav. Brain Res. *233*, 55–61. 10.1016/j.bbr.2012.04.045.
76. Paulus, M.P., Dulawa, S.C., Ralph, R.J., and Mark A Geyer, null (1999). Behavioral organization is independent of locomotor activity in 129 and C57 mouse strains. Brain Res. *835*, 27–36. 10.1016/s0006-8993(99)01137-3.

Figure 1. Map of the functional projections from barrel cortex to single SPNs.

A. Montage of a corticostriatal slice (left) and layout of the experiment (right). A SPN was recorded in the dorsolateral striatum while cortical neurons were photostimulated with LSPS. The grid of LSPS (blue) was postionned on the barrel cortex. GPe, globuls pallidus, external segment; IC, internal capsule; hipp. , hippocampus.

B. Example EPSCs recorded in two SPNs. Responses were evoked by the photorelease of glutamate at the sites indicated by letters a-c in the maps shown in C. Two repetitions are superposed (black and gray). Stimulus onsets are indicated by the vertical dashed lines (2 ms duration).

C. Examples of synaptic input maps for individual SPNs showing one or four clusters of input (cell 1 and 2, respectively). Each pixel of color indicates the peak amplitude of EPSCs detected within a 50 ms window after the stimulus onset. The different cortical layers are represented by solid white vertical lines on the left side of the map. Traces corresponding to the zones indicated by letters are shown in B.

D. Contribution of each cortical layer to the SPN innervation (n =101 cells, N = 54 mice). The 16 rows of the grid correspond to different cortical layers (Layer 2/3: 1-6; L4: 7-9; L5a: 10; L5b: 11-13; L6: 14-16). The horizontal dashed lines show the L5A borders.

E. Amplitude of SPN largest EPSCs as a function of their laminar origin. Median (red) and 25-75th percentiles (boxes). * indicates significant difference (Kruskal-Wallis p = 0.0003, Dunn-Sidak posthoc test, p = 0.0003).

F. Overlay of the sites in barrel cortex where stimulations evoked EPSCs in SPNs. The shades of magenda indicate the position of the SPNs (grey circles) along the medio-lateral axis in dorsal striatum (axis at the bottom, 0 is Refhor in the Methods; n = 101, N = 54). Light shades are for lateral cells. Sites in orange and green are the input fields of the two cells shown in B,C.

G. Position of the sites in cortex innervating SPN as a function of the SPN position in striatum. Zero on the x and y axis is the position of the vertical dashed line shown in F. Regression, R = 0.58 (n = 101, N = 54). The orange and green symbols are the two cells shown in B,C.

Figure 2. Excitatory neurons connecting individual SPNs are sparse and specific

A. Fraction of cells receiving inputs from 1 to 6 clusters of projections in barrel cortex. n = 101 cells, N = 54 mice. Clusters are defined as the ensemble of contiguous sites in the input map, collapsed along its vertical axis, whose stimulation evoked EPSCs.

B. Width of clusters of inputs, all cells combined. In inset, the width of clusters located in L5a. Median (red) and 25-75th percentiles (box). 192 clusters.

C. Left, Number of clusters of input in barrel cortex per SPN. Each dot is a cell, each line a slice. Only experiments with ≥ 2 recordings with input are shown. Right, three example slices with 3 or 4 recordings. The polygones are the stimulation sites evoking EPSCs, the boxes on top are the clusters generated from the collapsed input maps, the circles at the bottom the position of the SPNs on the horizontal axis. Recordings are color coded.

D. Width of the input field of SPNs in the barrel cortex (n = 101, N = 54).

E. Fraction of the input field, collapsed along its vertical axis, where stimulations evoked EPSCs in SPNs. Median (red) and 25-75th percentiles (box)

F. Fraction of the input field where stimulations evoked EPSCs in SPNs, as a function of the width of the input field. The input fields were not collapsed along the vertical axis here.

G. Sum of EPSCs when secondary adjacent (Adj.) clusters of projections were stimulated, relative to the the principal cluster EPSCs. 55 cells with ≥ 2 clusters are shown in inset.
H. Fraction of cells receiving inputs when stimulations were performed at various distances from their peak response in the input map.
I. Fraction of pairs of cells with 0 to 40 % overlap in their input maps. Cells in the pairs were in the same slice. In inset, the median (red) and 25-75th percentiles (box) of overlap across pairs. 70 pairs in 28 slices
J. Overlap in the input maps (symbols) and fraction of pairs with overlap in their input maps (stairs) for recordings performed in the same slice (red) or different slices (black and gray) as a function of the horizontal distance separating the cells in the pairs.

Figure 3. Strong similarities in the input fields of D1 and D2 SPN at the population level with some layer specificities.
A. Top, overlays of the sites in barrel cortex where stimulations evoked EPSCs in SPNs. The shades of red indicate the position of the D1 SPNs, and the shades of blue the position of the D2 SPNs along the medio-lateral axis in dorsal striatum. Light shades are for lateral cells. Bottom, position of the sites in cortex innervating each SPN as a function of the SPN position in dorsal striatum. R = 0.58 (D1, n = 47, N = 36) and 0.62 (D2, n = 54, N = 37).
B. Contribution of each cortical layer to the D1 SPN (red) and D2 SPN (blue) innervation.
C. Number of clusters in the input field of D1 and D2 SPNs. Median (thick line) and 25-75th percentiles (box)
D. Width of the input field of the D1 and D2 SPNs in the barrel cortex.
E. Amplitude of the sum EPSCs of D1 and D2 SPNs. Outliers were not shown for clarity (1 D1, 2 D2, 1.2-1.5 nA)
F. Top, Amplitude of the D1 and D2 SPN sum of EPSCs as a function of their laminar origin. Cells without inputs are not included. Outliers were not shown for clarity (3 D1, 2 D2, 350-700 pA). Bottom, fraction of cells with input for different laminar origins.
G. Sum of EPSCs evoked in D1 and D2 SPN when secondary adjacent (adj.) clusters of projections were stimulated, relative to the principal cluster EPSCs. Cells with ≥ 2 clusters; D1, n = 24; D2, n = 31.

Figure 4. The properties of D1 and D2 SPN input fields in barrel cortex vary in relation to the intrinsic behavioral biases of mice.
A. Traces, trajectories of mice in an open field, placed in the dark (13 are shown, 5 min). The side of the body, right or left, that mice exposed to the walls during thigmotaxis was tracked (RB and LB scanning) along with its speed mode. Traces in green, trajectories in the low speed mode (< 10 cm s-1). In orange, trajectories in the high speed mode (> 10 cm.s-1). All analysis were performed on the mouse trajectories by the border of the open field.
B. Matrices of Spearman correlation coefficients describing the relationships between properties of the D1 (left, N = 35) and D2 (right, N = 34) SPN input fields (lines) and features of thigmotaxis (columns). The green contours indicate the significant correlations with a false discovery rate (FDR) < 5 %. +, correlations signficantly different between D1 and D2, taking the absolute values of coefficients, with a FDR < 5%.
C. Relationship for the significant electrophysiology/behavior pair obtained with the D1 data set. Each point corresponds to a mouse.

D. Number of clusters innervating D1 SPNs as a function of the animal bias towards LB or RB scanning. *, D1 SPNs of mice with p. RB scanning ≥ 0.5 had significantly more clusters of inputs (p = 0.046, Welch's t-test).

E. % of recorded D1 SPNs without input in the barrel cortex (only cells from slices in which inputs were found are included). n = 31 and 41 cells for LB and RB biased mice.

F. D1 SPN input fields are not significantly larger in the barrel cortex of mice with p. RB scanning ≥ 0.50 (p = 0.18, Mann-Whitney) .

G. Superposed input fields (red shaded boxes) of D1 SPNs in right body-sided (top, p. RB scanning ≥ 0.51) and left body-sided mice (bottom, p. RB scan. ≤ 0.49). 16 cells each condition. The polygones indicate the location of the connected cortical cells; the circles at the bottom, the location of the SPNs in striatum.

H, I. Relationship for the two significant electrophysiology/behavior pairs obtained with the D2 data set. In blue, the correlation fit assuming a linear relationship between input field density and mean high speed during RB thigmotaxis (Pearson R = -0.59).

J. D2 SPN input field density as a function of the mean high speed of mice during LB thigmotaxis (i.e. when the ipsilateral body-side was exposed to walls). In blue, the correlation fit assuming a linear relationship (Pearson R = -0.46).

K. D2 SPN input fields are significantly larger in the barrel cortex of mice with a mean high speed > 18 cm/sec (18 is all mice median value; p = 0.0042, Mann-Whitney) .

L. Left, Superposed input fields (blue shaded boxes) of D2 SPNs in mice running in the OF (top, mean high speed > 20 cm.sec-1) and in mice exploring the OF slowly (bottom, mean high speed ≤ 18 cm.sec-1). 18 cells each condition. The polygones indicate the location of the connected cortical cells; the circles at the bottom, the location of the SPNs in striatum. Right, the input fields are aligned horizontally on their right extremity.

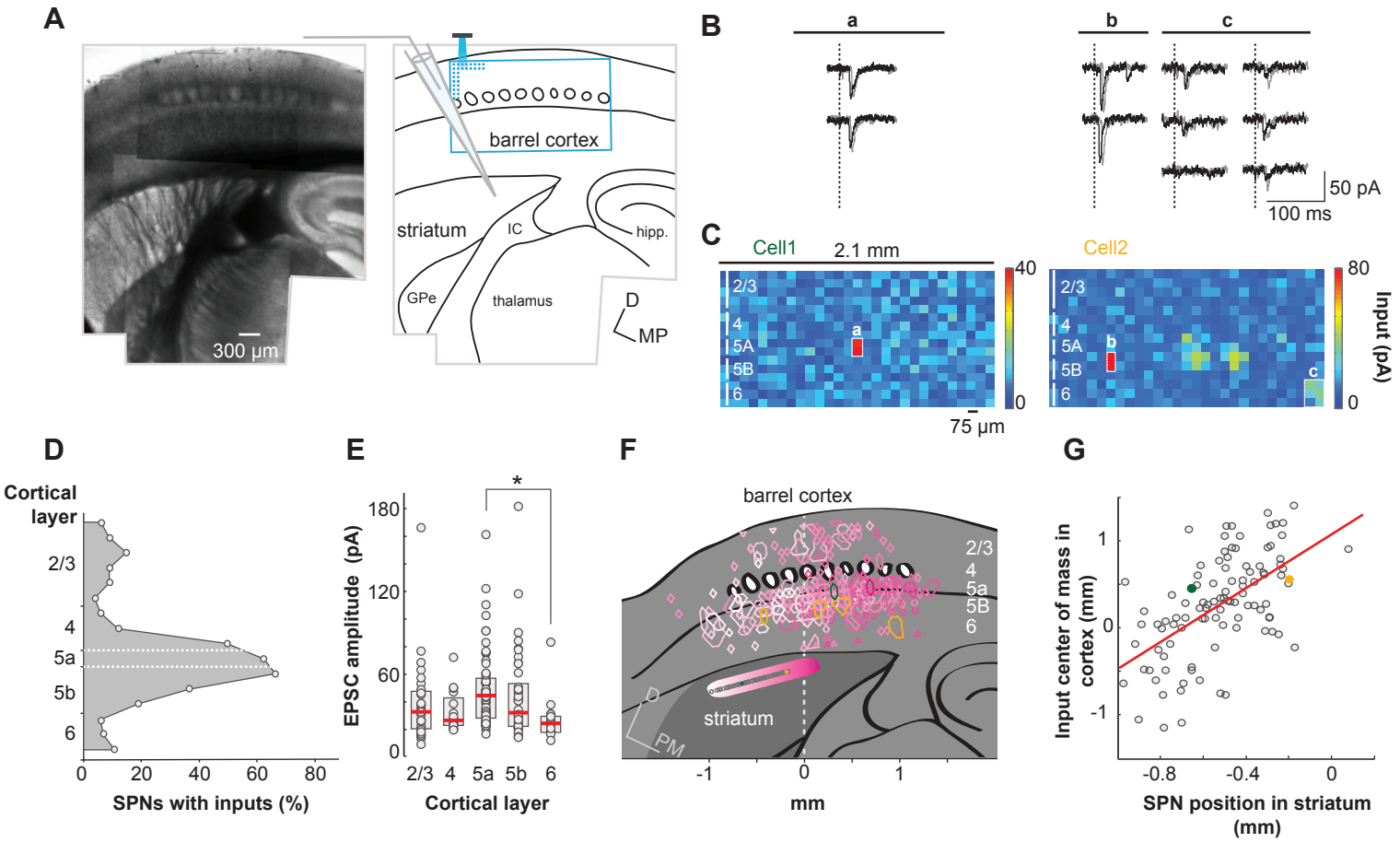
A
300 µm
barrel cortex
striatum
IC
hipp.
GPe
thalamus
D
MP
B
a
b
c
50 pA
100 ms
C
Cell1
2.1 mm
Cell2
2/3
4
5A
5B
6
40
0
80
Input (pA)
75 µm
D
Cortical layer
SPNs with inputs (%)
E
EPSC amplitude (pA)
Cortical layer
F
barrel cortex
striatum
PM
mm
G
Input center of mass in cortex (mm)
SPN position in striatum (mm)

Figure 1

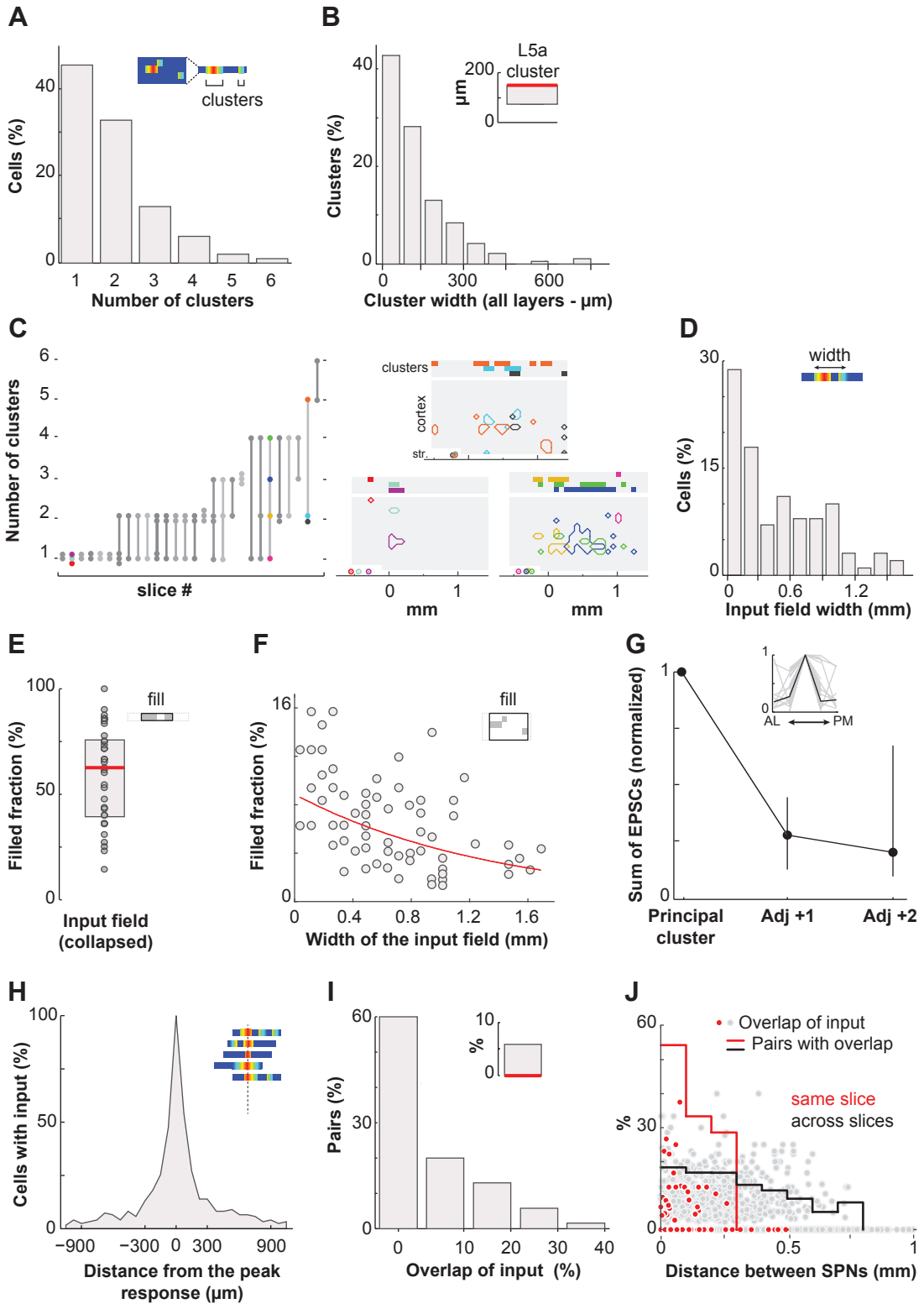
A
Cells (%)
clusters
Number of clusters
B
Clusters (%)
L5a
cluster
µm
Cluster width (all layers - µm)
C
Number of clusters
slice #
clusters
cortex
str
mm
mm
D
width
Cells (%)
Input field width (mm)
E
Filled fraction (%)
fill
Input field
(collapsed)
F
Filled fraction (%)
fill
Width of the input field (mm)
G
Sum of EPSCs (normalized)
AL
PM
Principal
cluster
Adj +1
Adj +2
H
Cells with input (%)
Distance from the peak
response (µm)
I
Pairs (%)
Overlap of input (%)
J
Overlap of input
Pairs with overlap
same slice
across slices
Distance between SPNs (mm)

Figure 2

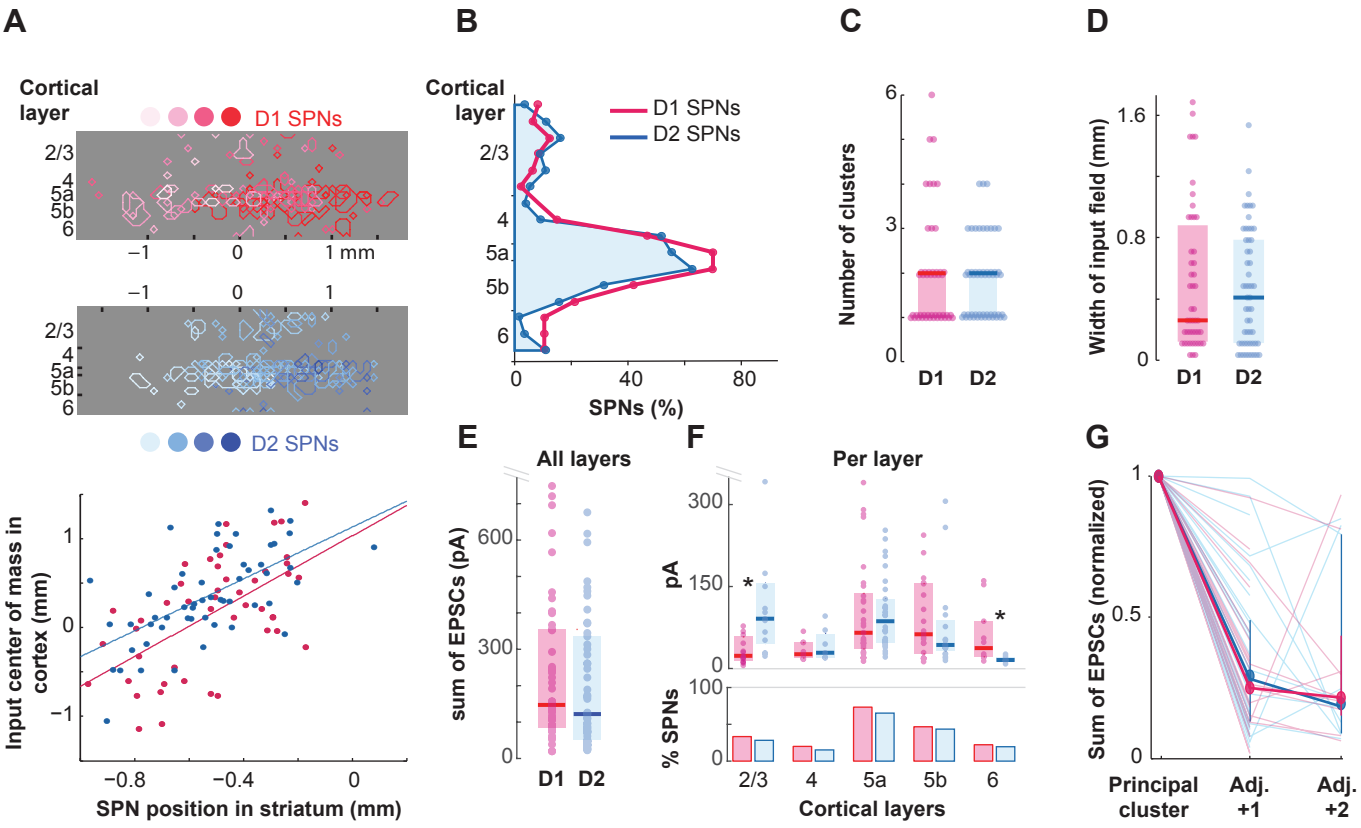
A
Cortical layer
D1 SPNs
2/3
4
5a
5b
6
−1
0
1 mm
D2 SPNs
Input center of mass in cortex (mm)
SPN position in striatum (mm)
B
Cortical layer
D1 SPNs
D2 SPNs
SPNs (%)
C
Number of clusters
D1
D2
D
Width of input field (mm)
E
All layers
sum of EPSCs (pA)
F
Per layer
pA
% SPNs
Cortical layers
G
Sum of EPSCs (normalized)
Principal cluster
Adj. +1
Adj. +2

Figure 3

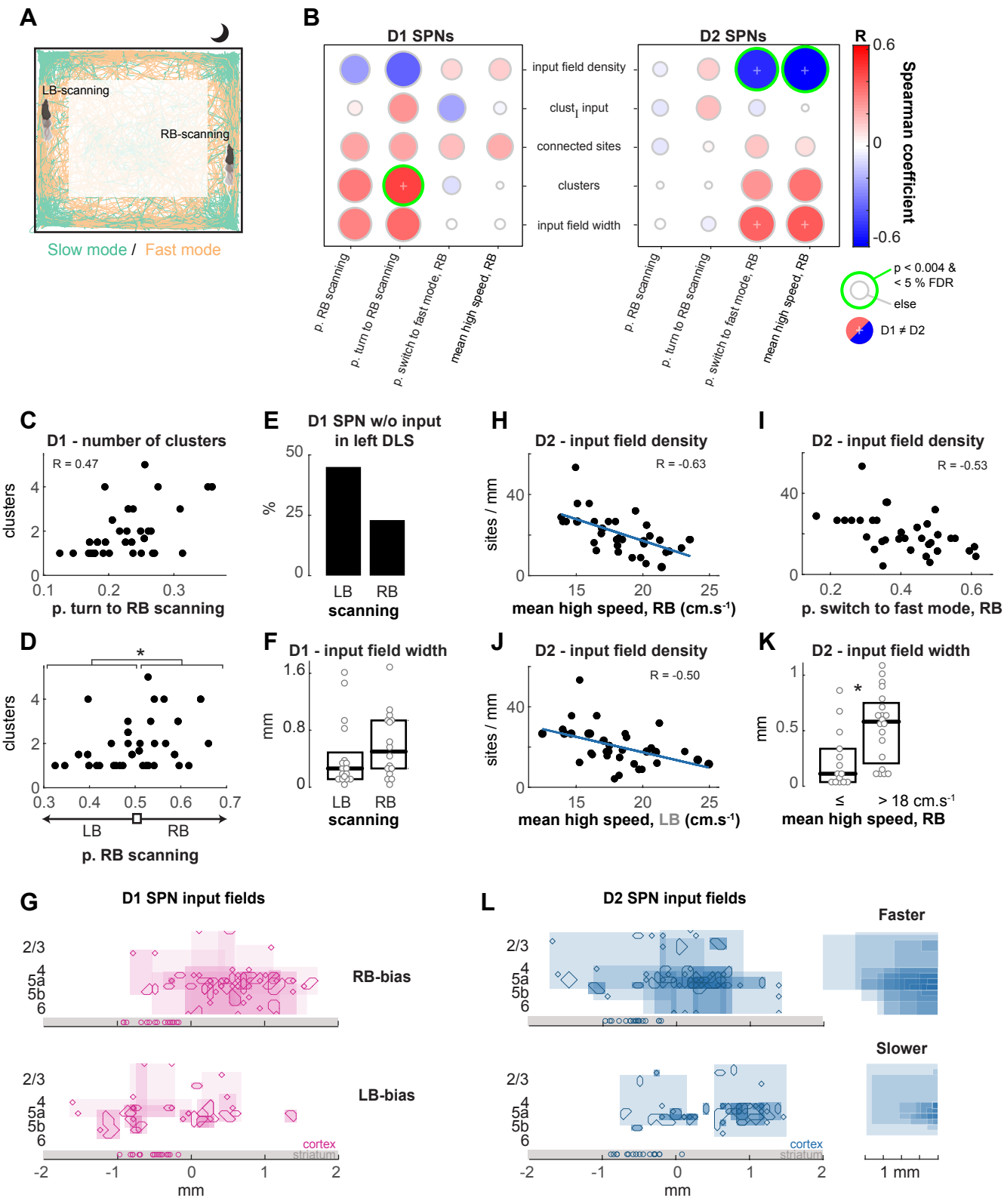
A
LB-scanning
RB-scanning
Slow mode / Fast mode
B
D1 SPNs
D2 SPNs
input field density
clust_I input
connected sites
clusters
input field width
p. RB scanning
p. turn to RB scanning
p. switch to fast mode, RB
mean high speed, RB
R
0.6
0
-0.6
Spearman coefficient
p < 0.004 & < 5 % FDR
else
D1 ≠ D2
C
D1 - number of clusters
R = 0.47
clusters
p. turn to RB scanning
E
D1 SPN w/o input in left DLS
%
LB
RB
scanning
H
D2 - input field density
R = -0.63
sites / mm
mean high speed, RB (cm.s-1)
I
D2 - input field density
R = -0.53
p. switch to fast mode, RB
D
clusters
LB
RB
p. RB scanning
F
D1 - input field width
mm
scanning
J
D2 - input field density
R = -0.50
sites / mm
mean high speed, LB (cm.s-1)
K
D2 - input field width
mm
≤
> 18 cm.s-1
mean high speed, RB
G
D1 SPN input fields
RB-bias
LB-bias
2/3
4
5a
5b
6
cortex
striatum
mm
L
D2 SPN input fields
Faster
Slower
1 mm

Figure 4

Supplemental Fig. 1 . Experimental conditions

A. Left, the corticostriatal slice generated from the Allen mouse brain reference atlas by the CutNII custom-angle slice visualization tool (G. Csucs). bf, barrel field. str, striatum. VPL, ventral posterolateral thalamic nucleus. VPM, ventral posteromedial thalamic nucleus. GPe, globus pallidus, external segment. Center, the section angles illustrated on a horizontal and longitudinal sections of the brain. Right, the section angle with respect to the orientations of the arcs and rows in the barrel field of the left hemisphere (Allen mouse brain atlas).

B. Excitation of two L5a pyramidal neurons evoked by LSPS. Glutamate was uncaged on a 8 x 8 (left) or on a 24 x 8 (right) - 50µm spacing grid while APs evoked in the cortical neuron positionned at the center of the grid (white triangle) was recorded in current-clamp mode, at the cell resting membrane potential. Traces with an action potential are in red.

C. Total number of APs evoked in the stimulation grid for L5 (left) and L2/3 (right) pyramidal cells in juvenile (juv, P22-30) and adolescent (ado, P31-41) mice. A higher stimulation intensity was used for stimulating the cortex in adolescent mice (25 mW instead of the standard -std - intensity, 20 mW), so that the total number of APs matched between the two age groups. L5, juv: number of cells, n = 22, number of mice, N = 9 ; ado std: n = 22, N = 13; ado high: n = 8, N = 5; L2/3, juv: n=16, N=3; ado std and high n = 10, N = 2; * indicates $p < 0.001$, Mann-Whitney.

D. Vertical (left) and horizontal (right) excitation profile of L5 pyramidal cells, in juveniles and adolescents combined (20 and 25 mW stimulation, respectively). Evoked APs were summed along each column (left) or each line (right) of the LSPS grid. Solid line, median. In gray, 25-75th percentiles. n=30, N = 14.

Supplemental Fig. 2 Behavioral parameters

A. Left, the lateralization indices of mice tested in two configurations are correlated. The sensory bias of the mice was assessed in a second task for 10 minutes in which they spontaneously cross a hole in a plate. The mouse was in the dark. It jumped to the edge of the hole (6 cm diameter, 3 cm high), scanned its contours, the outer surface of the plate, and the floor with their face and whiskers, and then stepped down. Created with BioRender.com. The center of mass of the mouse was tracked as it exited the hole. Purple traces, a mouse's trajectories when exiting to the RB side. Black traces, its trajectories when exiting to the LB side. Light gray traces, other trajectories before and after exiting the hole. Mice could enter the hole from either side, traces were realigned for clarity. Scale bar, 2 cm. Bottom inset, the trajectories aligned to the position of the mouse before it steps down. Right, the rate at which they chose to exit to their RB side is compared to their preferrence for the RB side during thigmotaxis in the open field (N = 11). Dashed line, identity line. Blue line, the fit with an intercept at 0.

B. The mean speeds of mice during thigmotaxis in two environments were correlated. Y axis, the mean speed of mice in a circular arena (30 cm diameter arena with a center rod). X axis, the mean speed of mice in the OF of the study. Mice were first tested in the OF (N = 61). Dashed line, identity line. Blue line, the fit with an intercept at 0.

C. Left, A bi-phasic distribution of speeds was observed in all mice (N = 78), from the fastest to the slowest (~15 per group), except for the slowest (blue). Fastest mice were more often in the high-speed mode and were on average faster in this mode compared to other mice. Dashed line, the cut-off between speed modes.

D. Tortuosity index of the trajectories inside the zones of OF, in low (green) and high speed (orange) mode. The tortuosity index is the actual distance traveled inside a zone over the optimal distance ratio - 1. Median (thick line) and 25-75th percentiles (box). Trajectories in corners were excluded. N = 78. Traces on the right are examples of these trajectories, aligned to one extremity (+). The mouse trajectories were in straight lines in the high speed mode and meandering in the low speed mode.
E. The high speed mode (orange) was dominant everywhere except in corners. The low speed mode (green) was seen at similar frequencies across the OF.
F. The mice differed in their propensity to be in the high-speed mode, but we could not link this to their anxiety level because they spent similar amounts of time in the center of the OF. Symbols, total time spent in the center of the OF as a function of the mouse average speed during the session. Thick line, median and box, 25-75th percentiles.
G. Cross-correlation matrix for the behavioral variables (left) and electrophysiological variables (right). At the bottom, the hierarchical dendritic trees.
H. Impact of spatial binning of the strip along the open field border and the detection of body side-changes. Increasing the size of the zones up to 28 cm linearly increased the measure of the probability that mice switched from LB to RB side while scanning the wall (right). This is expected because the probability that any zone contained a u-turn increased then. The measure reached a plateau when the size of zones exceeded the average length of the mice continuous runs ~ 50 cm (i.e. w/o change of direction; blue vertical line; 25-75th percentiles in cyan). Hence, a spatial binning of the OF border with zones 7 to 28 cm long was suitable for realiably detecting body side changes whereas longer zones led to an underestimation of the frequency of these changes as the probability of a zone containing more than one such event increased. White symbols, the size of the zones in the study, 11 cm.
I. The Spearman correlation coefficient for the D1 electrophysiology/behavior pair obtained with different spatial binnings of the OF (see G). Dashed line, the binning in the study. The correlation between the number of clusters in the D1 SPN input fields and the probability of a mouse switching from the LB to the RB side during thigmotaxis was stable for several spatial binnings, but decreased when the size of the zones exceeded the length of a continuous run (blue vertical line ~50 cm; 25-75th percentiles in cyan), i.e. when they were too long to detect all changes of body side.
J.Distributions of the speeds measured at each visit of a zone by the OF border for three different spatial binnings. In black, the distribution of the mouse speed with zones 11 cm long used for the rest of the study. Zones 11 or 14 cm long yielded a bi-phasic distribution of speeds. Longer zones (28 cm, light gray) did not allow the two-speed modes to be distinguished.
K. The Pearson correlation coefficients for two D2 electrophysiology/behavior pairs obtained with different cut-offs between the low and high speed modes. In dash, the cut-off in the study.

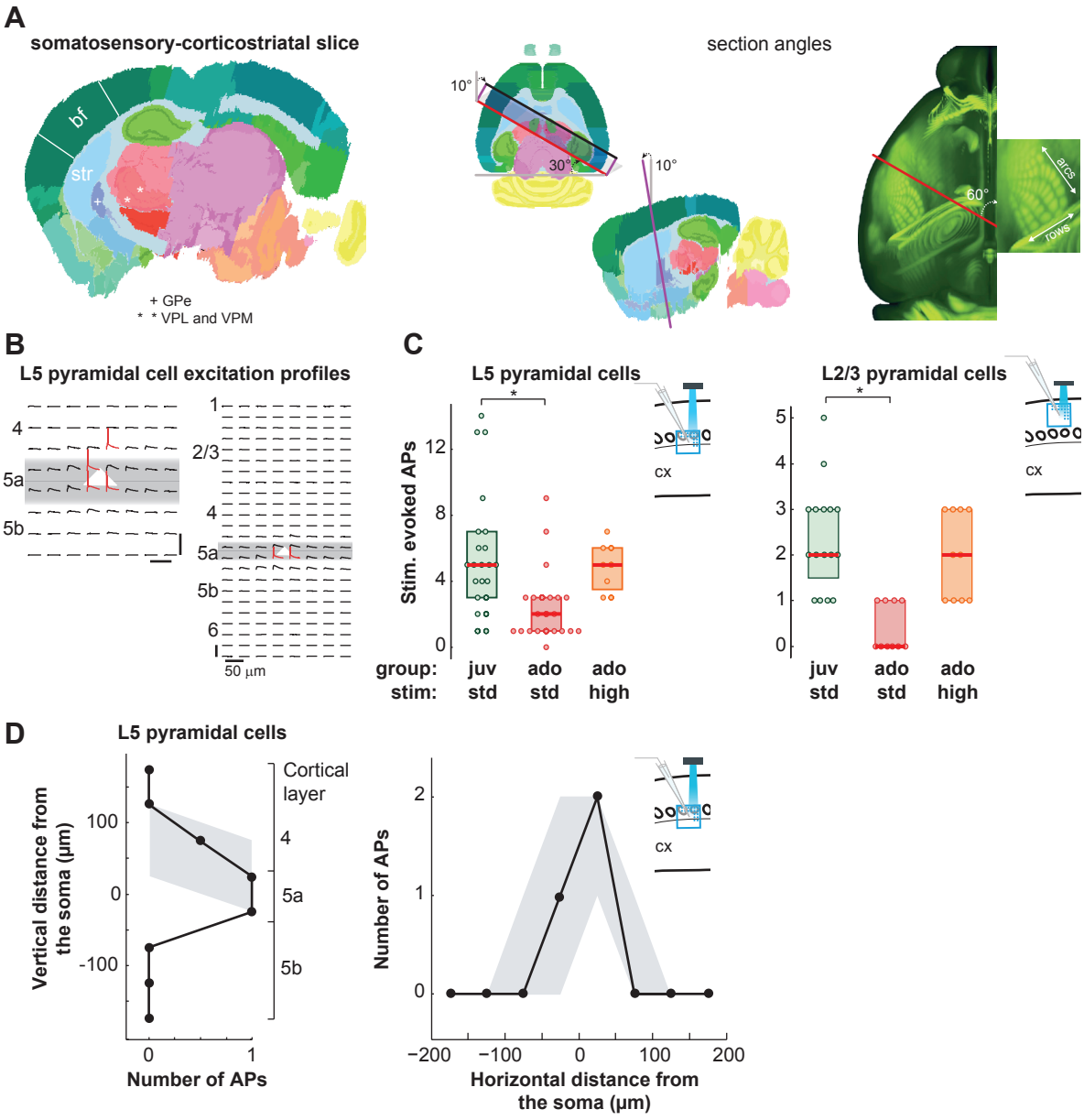

Supplemental Figure 1

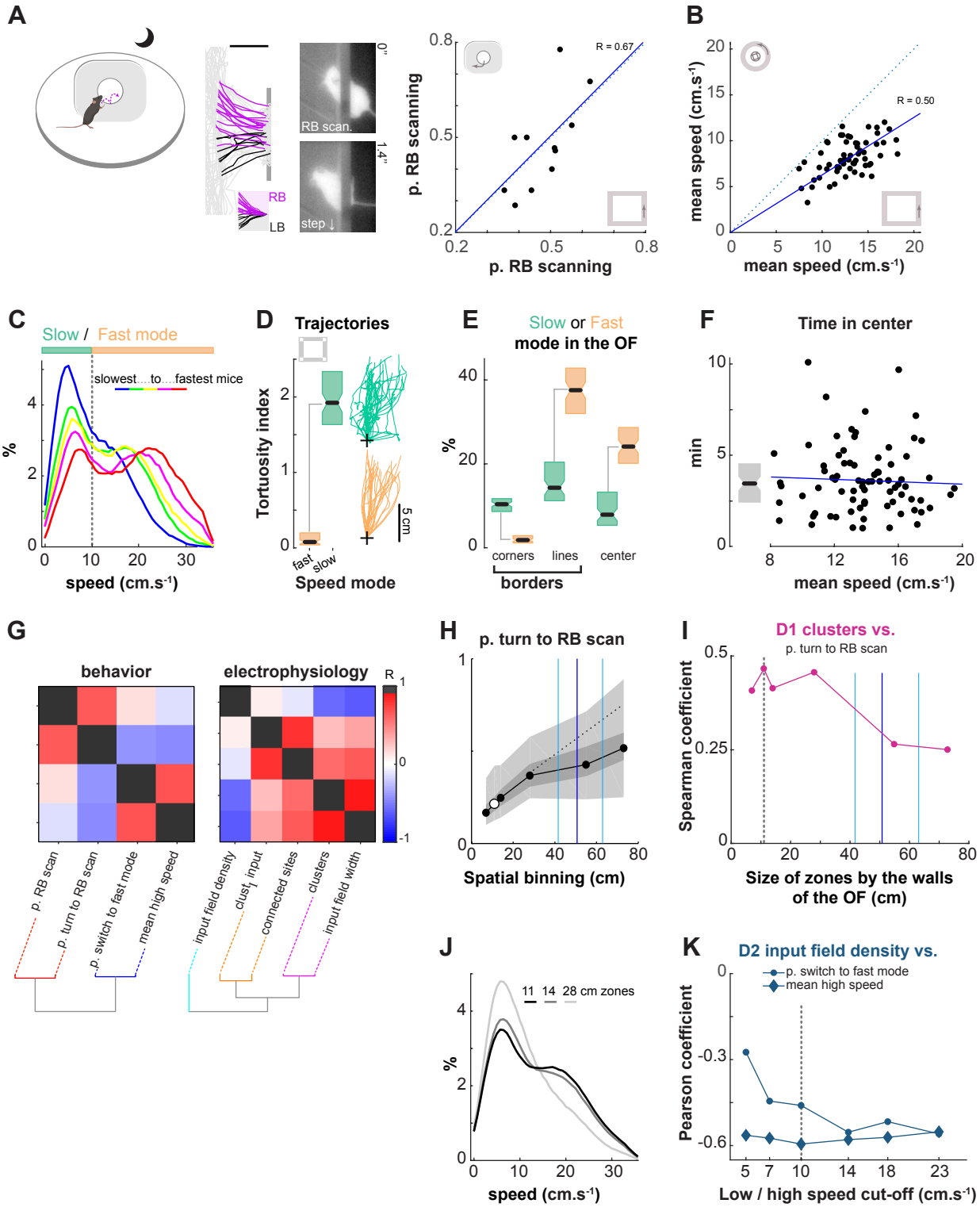

Supplemental Fig. 2